Performance improvement of on-chip integrable terahertz microbolometer arrays using nanoscale meander titanium thermistor

Amit Banerjee, Hiroaki Satoh, Durgadevi Elamaran, Yash Sharma, Norihisa Hiromoto, and Hiroshi Inokawa

View Online   Export Citation   CrossMark

Performance improvement of on-chip integrable terahertz microbolometer arrays using nanoscale meander titanium thermistor

Amit Banerjee,[1,2] [ID] Hiroaki Satoh,[1] [ID] Durgadevi Elamaran,[3] Yash Sharma,[3] Norihisa Hiromoto,[4] and Hiroshi Inokawa[1,a)] [ID]

AFFILIATIONS

[1]Research Institute of Electronics, Shizuoka University, 3-5-1 Johoku, Naka-ku, Hamamatsu 432-8011, Japan
[2]Department of Electrical and Computer Engineering, National University of Singapore, 21 Lower Kent Ridge Rd, Singapore 119077
[3]Graduate School of Science and Technology, Shizuoka University, 3-5-1 Johoku, Naka-ku, Hamamatsu 432-8011, Japan
[4]Graduate School of Integrated Science and Technology, Shizuoka University, 3-5-1 Johoku, Naka-ku, Hamamatsu 432-8011, Japan

Note: This paper is part of the Special Topic section "Advances in Terahertz Solid-State Physics and Devices" published in J. Appl. Phys. **125**(15) (2019).
[a)]**E-mail:** inokawa.hiroshi@shizuoka.ac.jp

ABSTRACT

In this study, uncooled antenna-coupled microbolometer arrays were fabricated to detect terahertz waves by using nanoscale meander-shaped Ti thermistors with design widths of DW = 0.1 and 0.2 μm, respectively, on SiO_2 and SiN_x substrates. Each unit device with a thermistor with DW = 0.1 μm yielded double the electrical responsivity (787 V/W) of unit devices with thermistors with DW = 0.2 μm (386 V/W) at the maximum allowable bias current (I_b = 50 for DW = 0.1 μm and 100 μA for DW = 0.2 μm, respectively). However, the calculated noise-equivalent power (NEP) of unit devices with thermistors with DW = 0.1 μm was 1.85×10^{-10} W/$\sqrt{\text{Hz}}$ at I_b = 50 μA and 1.58×10^{-10} W/$\sqrt{\text{Hz}}$ at I_b = 100 μA for unit devices with thermistors with DW = 0.2 μm. Hence, the reduction in DW did not lead to an improvement in NEP. This study validates our previous investigation into the effect of width on such device parameters such as the temperature coefficient of resistance (TCR) and resistivity in the context of device miniaturization. The smaller grain size in thinner metal interconnects (thermistors) can be linked to the lower TCR and increased resistivity of the devices. Thus, the enhancement in responsivity in the design was largely due to the nanoscale meander design that, however, was detrimental to the noise response of the devices. These devices with nanoscale Ti meander thermistors deliver high responsivity in unit devices with scope for further miniaturization and have significant potential for application as on-chip integrable detector arrays.

I. INTRODUCTION

Research on modern thermal radiation detectors originated in homeland security and surveillance needs for night vision. Recent advancements in thermal detector technology, combined with semiconductor device processing and materials science for on-chip integrable devices, offer avenues for application with significant potential.[1] Terahertz (THz) technology involves efforts to harness the power of thermal radiation (~300 GHz–3 THz) and offers remarkable potential for application. The region of electromagnetic frequency around ~1 THz is the most interesting for applications of remote and nondestructive sensing. Electromagnetic waves with shorter wavelengths struggle to penetrate matter and are, hence, not useful for analyzing the interior of materials. THz waves yield high-resolution images compared with millimeter waves and yet are nonionizing and do not trigger harmful chemical reactions because of their low photon energy. Moreover, in the THz region, it is possible to detect molecular vibrations related to weak inter-molecular coupling. THz waves are useful in a wide range of

applications, e.g., ultrahigh-speed wireless communication, biomedical diagnosis (screening tooth decay and skin cancer, diagnosing tumors protein, analyzing DNA and genes), drug discovery,[2,3] environmental monitoring, homeland security (noncontact inspection of explosives, poison gas clouds, hidden weapons, T-ray vision peering through walls),[4–6] analysis of materials (defects in tile materials of space shuttles, inspection of imperfections), and food diagnostics (foreign substances in foods).[7] This spectral band has been used in ground or space radio telescopes in the context of remote sensing to investigate the chemical compositions of interstellar materials and mediums as well as planetary atmospheres.[8,9] Some significant breakthroughs have been reported in high-power THz sources in the past decade,[10] including uncooled detectors[11–13] and simultaneous (real-time) imaging.[14,15] Further innovation is under way in applications with powerful sources and competent detectors to develop commercially viable high-speed sensing and communication systems that are superior to prevalent solid-state devices and compatible with flexible electronics.[16–20] The THz research field offers a diverse range of discoveries and applications, but it is important to study perspective THz sources, detectors, optical elements for sensitivity, and speed of measurements for commercially viable products.

Photon detectors and thermal detectors are the two major types of detectors for the far-infrared and THz regions. The microbolometer, as a THz detector, does not require additional cryogenic support like photon detectors.[21] However, its detectivity suffers from thermal noise at room temperature, and it faces other performance issues, such as an extended response time, self-heating (under bias),[22,23] and dependence of its responsivity on a susceptible thermistor (sensor) material.[24] These issues should be addressed for further improvement of the device. The basic design of a microbolometer consists of (a) an absorber, to receive THz radiation and transfer it to the other part, and (b) a thermistor, which heats up causing a change of resistance, which is further calibrated for sensing. Large absorbers at longer ranges of wavelength like THz render structural sustainability challenging with adequate thermal isolation. In such conditions, an antenna-coupled microbolometer has been found to be technologically feasible.[25] The thermistor and the heater in a microbolometer with electrical separation need to be independently optimized and thermally coupled for higher sensitivity.[22,26] Our electromagnetic simulation of an antenna-coupled heater demonstrates that a reasonable improvement in performance is expected for a microbolometer with an optimum heater resistance. This helps maximize power transfer between the antenna and the heater, as THz irradiation-induced current in the antenna flows into the heater, at the center of the antenna.[27] One figure of merit of a microbolometer is its responsivity, which is defined as the ratio of the output voltage to input power. A high responsivity relaxes the requirement for the readout circuit, i.e., the input-referred noise of the preamplifier can be larger, leading to a smaller footprint and power consumption of the preamplifier. Another important figure of merit in the current discussion, the noise-equivalent power (NEP), for the microbolometer is obtained by measuring the electrical noise generated by the detector. Note that responsivity is directly proportional to the temperature coefficient of resistance (TCR), and NEP is inversely proportional to the TCR of the thermistor material. Hence, the TCR of the thermistor is the most important parameter

in the design of a microbolometer. Metallic thermistors, e.g., composed of bismuth (Bi) and titanium (Ti), have relatively small bulk TCR than high-TCR materials, e.g., vanadium oxide (VO_x) and amorphous silicon (a-Si). However, metallic thermistors feature reduced noise (mainly shot and thermal noises);[28] hence, the device performance has a direct advantage in case of relatively higher TCR achieved in any design. This is not the case with VO_x and a-Si. Ti is used for the thermistor–heater material considering its (i) low thermal and electrical conductivity, (ii) invulnerability to electromigration, and (iii) low flicker noise.[28,29] Our previous attempts to fabricate an uncooled antenna-coupled microbolometer in the 1-THz band resulted in moderate responsivity of ∼90 V/W and NEP of ∼4.6 × 10^{-10} W/Hz$^{1/2}$.[26,27,30,31] From an examination of the scaling trend of integrated thermistor–heater system, it was found[31] that the cutoff frequency improves by downscaling the length. However, responsivity reduces with the reduction in the length of the thermistor while keeping the other dimensions fixed. A meander structure is most appropriate for relaxing such a trade-off relationship. From our electrothermal simulation of an integrated Ti heater–thermistor system, the expected electrical responsivity for a meander shape is approximately four times higher than that of a microbolometer with a straight-line thermistor.[31]

In the present design of the microbolometer, the meander-shaped thermistor with increased effective length has higher electrical resistance, resulting in enhanced responsivity. However, the current design encounters reduced TCR because of the utilization of Ti thermistors with narrow design width (DW = 0.1 μm or 0.2 μm), which yield one-third of the TCR of bulk Ti.[32] Although metal conductors are widely used in ultra-large-scale integrated circuits (ULSI), interconnects at the size scale ∼ mean free path of the conduction electrons suffer from size effects that adversely influence their electrical properties. The phenomenon of the change in the electrical parameters (reduced TCR, increased resistivity) of a thin metal interconnect is called the narrow-width effect. In the quest for miniaturization, the consequence of the narrow-width effect on device performance, e.g., in terms of responsivity, is examined for microbolometers with meander-structured nanoscale Ti thermistors in this study. To the best of the authors' knowledge, this is the first study to investigate an enhancement in the responsivity of a microbolometer using nanoscale meander thermistors compatible with prevalent semiconductor fabrication technology for a comprehensive understanding of the narrow-width effect in metal nanowires.

II. METHODS OF FABRICATION AND CHARACTERIZATION

The fabricated microbolometers were composed of an integrated heater/thermistor/half-wave dipole gold (Au) antenna with a titanium (Ti) heater, a SiO_2/SiN_x interlayer, and a Ti thermistor on a substrate (SiO_2/SiN_x). The thicknesses of the antenna, heater, interlayer, and thermistor were 200, 100, 100, and 50 nm, respectively. In the current design, the microbolometer arrays were equipped with a meander-shaped Ti thermistor, with a DW as small 0.1 and 0.2 μm, fabricated by electron beam lithography. The design of the meander of the thermistor led to a longer effective length that increased electrical resistance and, hence, responsivity. Note that the heater was

stacked on the thermistor but electrically isolated by a thin interlayer. The length and width of the heater were fixed at 11 and $2.1\,\mu m$, respectively, to ensure impedance matching with the half-wave dipole antenna. The microbolometer arrays consisted of 16 unit microbolometer devices, each of which was equipped with an integrated heater/thermistor/half-wave dipole antenna designed for 1 THz range. The characteristics of these devices were investigated at room temperature (300 K). As the current design is based on our previous investigation into developing these fine-patterned devices, the interested reader can refer to the relevant studies for the steps of processing and related discussion.[25,30–34] Electron micrographs were taken with an analytical JEOL JSM-7001F field-emission scanning electron microscope (FE-SEM). The electrical measurements for these devices were made with a low-temperature prober equipped with an Agilent 4156C precision semiconductor parameter analyzer. To characterize the TCR using the slope of resistance plotted against temperature, five temperatures from 300 to 240 K were used. The responsivities of these devices were measured by applying AC electrical power up to $5\,\mu W$ at a frequency of 10 Hz. The output of the thermistor was measured by a lock-in amplifier, with the maximum bias current limited to $50\,\mu A$ for DW = $0.1\,\mu m$ and $100\,\mu A$ for DW = $0.2\,\mu m$. The voltage noise was measured for the devices using the temperature-controlled prober, Nagase Techno-Engineering Grail 21-205-6-LV-R, with different bias currents (I_b) of the thermistor. The output noise voltage over a frequency range of 1 Hz–100 kHz was recorded by the Agilent 35670A FFT dynamic signal analyzer. Note that the capacity of the spectrum analyzer to measure low-amplitude signals was restricted by noise produced inside the analyzer. Hence, to attain maximum sensitivity, a preamplifier with low noise and high gain should be used. A DL Instruments' model 1201 low-noise voltage preamplifier with a maximum gain of ×10 000 and noise of less than $15\,nV/\sqrt{Hz}$ at 10 Hz was used to improve the sensitivity of the spectrum analyzer. The input from the microbolometer and the output of the preamplifier were AC-coupled to avoid overdriving the spectrum analyzer input as a result of DC offset caused by the bias current (I_b).

III. RESULTS AND DISCUSSION

This study is based on insights from our past research,[25,30–34] in the quest to understand the narrow-width effect, i.e., the detrimental effects of nanoscale widths on the TCR and resistivity (ρ) of metal interconnects (in this case, the thermistor) in the context of device miniaturization. A detailed study has been conducted on the variations in TCR and resistivity (ρ) as devices are miniaturized and squeezed by reducing various elements, including design width DW (more specifically, actual width or average measured width, AMW) for two substrates with straight-line thermistors.[34] The TCR and resistivity of the devices provided a good fit with the empirical formulas (1) and (2) and were found to hold well for all devices irrespective of the substrate (with AMW in nanometers, ρ in ohm meters, and TCR in percent per kelvin),[34]

$$\text{Ti on SiO}_2: \text{TCR} = 4.16 \times 10^{-02}\ln(\text{AMW}) - 8.54 \times 10^{-02}, \quad (1)$$

$$\text{Ti on SiN}_x: \text{TCR} = 3.64 \times 10^{-02}\ln(\text{AMW}) - 5.43 \times 10^{-02}, \quad (2)$$

$$\text{Ti on SiO}_2: \text{Resistivity } (\rho) = 6.837 \times 10^{-06}(\text{AMW})^{-0.2869}, \quad (3)$$

$$\text{Ti on SiN}_x: \text{Resistivity } (\rho) = 8.75 \times 10^{-06}(\text{AMW})^{-0.3260}. \quad (4)$$

Hence, for the current design based on the empirical equations, a device with the following specifications was used:

- Ti (on SiN$_x$/SiO$_2$/Si),
  - AMW = $0.2\,\mu m$: TCR = 0.138 %/K, ρ = 15.5×10^{-7} ohm m;
  - AMW = $0.1\,\mu m$: TCR = 0.113 %/K, ρ = 19.4×10^{-7} ohm m.
- Ti (on SiO$_2$/Si),
  - AMW = $0.2\,\mu m$: TCR = 0.135%/K, ρ = 14.9×10^{-7} ohm m;
  - AMW = $0.1\,\mu m$: TCR = 0.106%/K, ρ = 18.2×10^{-7} ohm m.

Note that the narrow-width effect due to a change in DW from 0.2 to $0.1\,\mu m$ for Ti (on SiN$_x$/SiO$_2$/Si substrate) led to a reduction of 22% in TCR while ρ increased by a factor of 1.25, whereas for Ti (on SiO$_2$/Si substrate) led to a reduction of 27% in TCR while ρ increased by a factor of 1.22.

For the present layout of the microbolometer, the design widths of the thermistor were DW = 0.1 and $0.2\,\mu m$, and its length could be varied to 48.7 or $89.5\,\mu m$. This was implemented by a sophisticated design (pattern) of the thermistor, i.e., a meander shape. The meander shape had a longer effective length, consequently higher resistance, and hence enhanced electrical responsivity. Figure 1(a) shows the variation in the actual width (AMW: average measured width), with respect to the DW of titanium (Ti) thermistor lines on two different substrate materials with a fixed length ($100\,\mu m$) and height ($0.05\,\mu m$), which follows linear relations up to 50 nm. However, noticeable differences between the AMW and DW were observed for the region of DW ∼ $0.1–0.2\,\mu m$ (100–200 nm), which is important in the current design layout. Due to this discrepancy between actual width and design width, TCR and resistivity were calculated using the average measured width (AMW) through scanning electron microscopy (SEM) instead of design width (DW). Furthermore, Fig. 1 shows the optical microscope (OM) [Fig. 1(b)] and SEM images of two of the test devices fabricated for the electrical measurement of TCR and ρ, with meander thermistors with DW = $0.1\,\mu m$ [Fig. 1(c)] and $0.2\,\mu m$ [Fig. 1(d)], with different pitch distances (PD = $0.2–0.28\,\mu m$) at a fixed length (L = $100\,\mu m$) and height (H = $0.05\,\mu m$). Figure 1(e) shows the variation in TCR and ρ with the change in the pitch of the thermistor for meander structures on two different substrates. Furthermore, the authors' examination of the correlation between enhanced resistivity and the lowering of TCR with a reduced AMW[34] showed that a reduction in wire pitch in the meander structure reduces ρ but increases TCR. Hence, for a high-TCR value, a pitch of $0.2\,\mu m$ was selected as the pitch of the thermistor for the fabrication of the microbolometer arrays. The thermistor widths DW = $0.1\,\mu m$ and $0.2\,\mu m$ were used for the current design layout for the fabrication of uncooled antenna-coupled THz microbolometer arrays for further investigation.

The authors conducted[34] a comprehensive study on electron backscatter diffraction (EBSD) of Ti lines with widths ranging on the nanometer scale, with detailed information on the grain orientations, sizes, and so on of the crystals. For a Ti film ($150 \times 150\,\mu m$) and thin
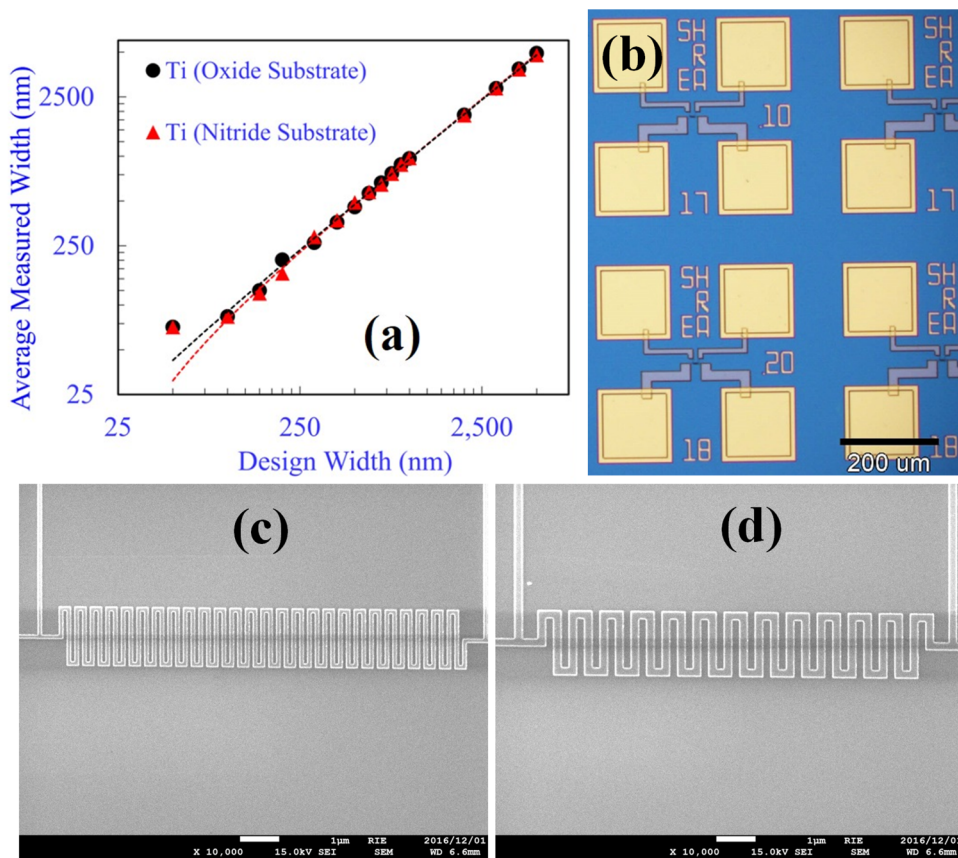
FIG. 1. (a) shows the relationship between actual width (AMW) and design width (DW) of thermistor lines on various substrates. (b) displays an optical microscope with FE-SEM micrographs of two test devices fabricated for electrical measurements of TCR and ρ, with meander thermistors with DW = 0.1 μm (c) and 0.2 μm (d). (e) shows the variation in TCR and ρ with the change in thermistor pitch for meander structures on different substrates.
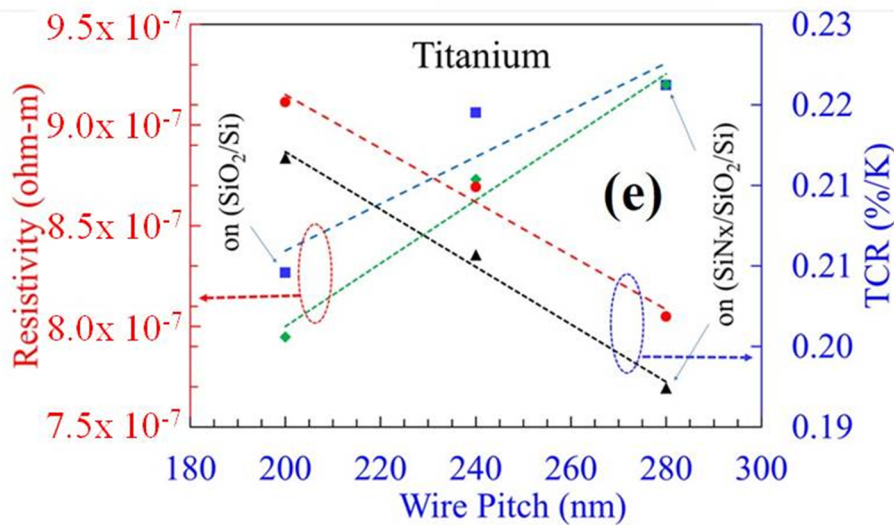
Ti nanowires with DW = 0.1 μm, no fixed or single-grain orientation was found. A cause of this feature might have been that the orientation and grain size of the crystal largely depend on the synthesis temperature of the thin film or metal lines being studied. The room-temperature synthesis of the thin Ti films or metal thin wires by vacuum evaporation and further lift-off process may give rise to random crystal orientations. Hence, the possibility of a particular crystal orientation contributing to the narrow-width effects in the electrical parameters can be eliminated in this investigation, which corroborated the results of the EBSD.[34] Rather, it is predicated that
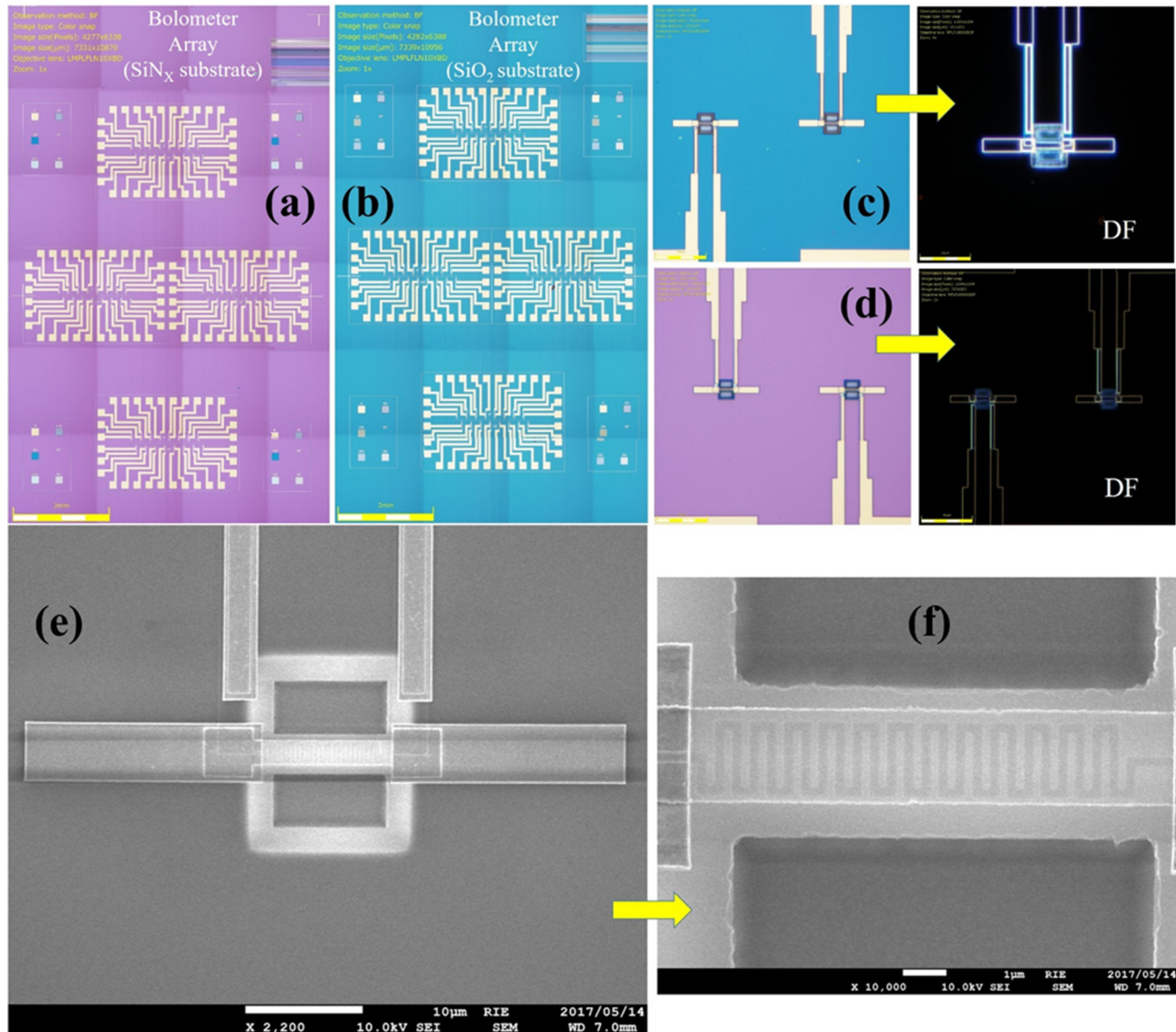
FIG. 2. (a) and (b) Optical microscope (OM) image of Ti uncooled antenna-coupled THz microbolometer arrays with DW = 0.1 and 0.2 μm on SiN$_x$ and SiO$_2$ substrates. (c) and (d) Enlarged OM image of a set of microbolometers with dark field OM. (e) and (f) FE-SEM enlarged view of a microbolometer device demonstrates the heater and the meander-structured thermistor floating above the cavity.

the reduction in TCR with the enhancement of resistivity is linked to the miniaturization of grain size as metal interconnects are squeezed (reduced DW). This might be evident from the FE-SEM and EBSD results linked to the electrical parameters (TCR and ρ). It is also expected that the conventional size effect due to enhanced surface scattering also contributed, but this is beyond the scope of the current discussion.

Figure 2 shows the uncooled antenna-coupled THz microbolometer arrays on two substrates along with an enlarged view of a microbolometer device and its meander structure floating on a cavity. The two types of microbolometer arrays were constructed

with a major difference in the length and width of the meander structure of the Ti wire:

TYPE 1: Ti thermistor length L_{th} = 48.7 μm, Ti meander thermistor DW_{th} = 200 nm,
- Ti heater L_h = 11.2 μm, heater width W_h = 2.1 μm, Au antenna, L_{ant} = 52 μm, W_{ant} = 5.2 μm;

TYPE 2: Ti thermistor length L_{th} = 89.5 μm, Ti meander thermistor DW_{th} = 100 nm,
- Ti heater L_h = 11.5 μm, heater width W_h = 2.1 μm, Au antenna, L_{ant} = 52 μm, W_{ant} = 5.2 μm.

Figures 2(a) and 2(b) show the optical microscope (OM) image of the Ti uncooled antenna-coupled THz microbolometer arrays with DW = 0.1 and 0.2 μm on SiN$_x$ and SiO$_2$ substrates. Figures 2(c) and 2(d) show a pair of unit microbolometer devices with dark field OM, where the meander structure of the thermistor is visibly suspended on a cavity because of the scattering from the edges of the cavity on the dark field images. The enlarged FE-SEM of a unit microbolometer [Figs. 2(e) and 2(f)] gives a clear view of the thermistor with a meander structure on top of the heater, suspended on top of the cavity for thermal isolation. Of the two sets of identical device arrays, one was used to reconfirm the material parameters (TCR, resistivity), while the other two were used for optical THz measurement.

Given that there was no remarkable difference in the material properties of the substrates, electrical responsivity measurement and frequency response with different bias currents for the thermistor are discussed for the SiO$_2$ substrate only. Moreover, optical responsivity with a THz source is currently being investigated and is expected to be proportional to the electrical responsivity discussed here. This report deals with the improvement in the electrical performance of the devices considering the authors' previous results or related devices, along with a correlation of the device parameters with the narrow-width effect of thin metal meander thermistors.

The authors have previously reported[34] the importance of higher responsivity (R_V) in microbolometer devices because the THz signal can be very low. R_V in units of V/W is defined as follows:

$$R_V = I_b \frac{dR_D}{dP_{in}}, \qquad (5)$$

where I_b is the DC bias current through the thermistor and $\frac{dR_D}{dP_{in}}$ is the change in the resistance of the detector (due to the power consumption of the heater).

Considering I = amplitude of an alternating heater current, the average input power is

$$P_{in}(ave) = \frac{P_{in}(peak)}{2} = \frac{I^2 R_0}{2},$$

where R_0 is the room temperature (T_0) heater resistance.

Now, the root mean-square output voltage of the bolometer is

$$V_{out}(RMS) = \frac{V_{out}(peak\ to\ peak)}{2\sqrt{2}}.$$

The bolometer's responsivity is

$$R_V = \frac{V_{out}(RMS)}{P_{in}(ave)}. \qquad (6)$$

The analysis can further be extended to[30]

$$R_V = I_b \frac{dR_D}{dP_{in}} = K\, I_b\, R_{th} \alpha_{th}. \qquad (7)$$

Here, I_b is the DC bias current through the thermistor, R_{th} is the thermistor resistance, α_{th} is the TCR of a thermistor, and K is

the proportionality constant depending on the material characteristics of the thermistor. It is evident that the slope of the input power against the output voltage from Eqs. (5)–(7) for the microbolometer gives the electrical responsivity (R_V). From the equations above, R_V is proportional to bias current (I_b), resistance, and TCR of the thermistor.

The relationships between responsivity (R_V) and physical parameters other than the dimensions of features of the device are also affected by the various limiting mechanisms. For example, the capacity of thermistors to handle large current without breaking depends on[30,35–37] Joule heating, electromigration failures (current density limits), breakdown of bias-induced electric field, unstable detector operation, heat loss by thermistor and heater voltage terminal leads, and sharp heating in a suspended thermistor floating above the cavity (for a suspended thermistor, resistance increases linearly with the square of the applied current and is proportional to resistors length).

To calculate the input power to the devices, Fig. 3(a) gives the input–output voltage response of the heater for microbolometer devices with thermistors of width DW = 0.2 μm (a) and 0.1 μm (b). The electrical responsivity of the microbolometers is shown for different bias currents to the thermistor with DW = 0.2 μm (b) and 0.1 μm (c). The electrical frequency response of both microbolometers devices is given in Fig. 3(d). The maximum current (and voltage) across the thermistor was considered well within the limit and could change the resistance in the thermistor by 3% through heating.

For the given microbolometers, TCR, resistivity, and the resistance of the thermistor were estimated according to the following parameters by considering Eqs. (1) and (3):

Ti (on SiO$_2$/Si),
DW = 200 nm: TCR = 0.135 %/K, ρ = 14.9 × 10^{-7} ohm m;
Resistance R ~ 6500 ohm (considering L = 48.7 μm, H = 55 nm)
DW = 100 nm: TCR = 0.106 %/K, ρ = 18.2 × 10^{-7} ohm m;
Resistance R ~ 29 500 ohm (considering L = 89.5 μm, H = 55 nm)

Based on the above, the expected ratio of responsivities for DW = 0.1 and 0.2 μm is

$$\frac{R_{V0.1}}{R_{V0.2}} = \frac{I_{b0.1}\, R_{th0.1} \alpha_{th0.1}}{I_{b0.2}\, R_{th0.2} \alpha_{th0.2}}$$
$$= \left(\frac{50}{100}\right) \times \left(\frac{29\,500}{6500}\right) \times \left(\frac{0.106}{0.135}\right) = 1.78. \qquad (8)$$

However, experimentally from Fig. 3, the ratio is

$$\frac{R_{V0.1}}{R_{V0.2}} = \left(\frac{787.5}{386.7}\right) = 2.03. \qquad (9)$$

The unit microbolometer devices with the thermistor with DW = 0.1 μm had twice the electrical responsivity of unit devices with the thermistor with DW = 0.2 μm at the maximum permissible current. Note also that unit devices with the thermistor with DW = 0.1 μm operated at half the bias current of devices with the thermistor with DW = 0.2 μm. Resistance in Eq. (8) might have been overestimated because we used DW instead of AMW, which
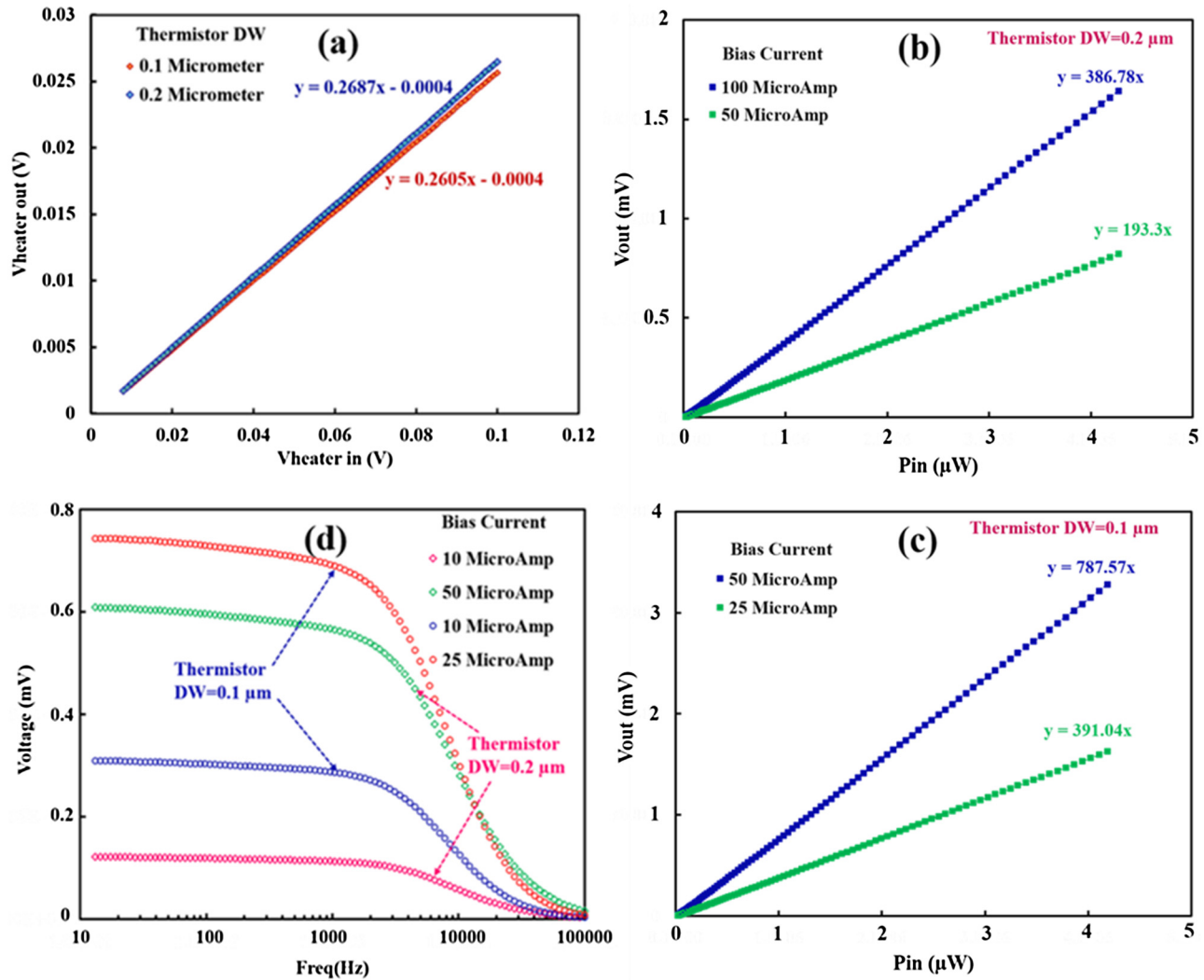
FIG. 3. (a) Input and output responses of the heater voltage for microbolometers with thermistor DW = 0.2 μm and 0.1 μm, respectively. Electrical responsivity on different bias currents to thermistor at frequency = 10 Hz, for microbolometers with thermistor DW = 0.2 μm (b) and 0.1 μm (c). (d) Frequency response for the above microbolometers.

was lower. From Eqs. (8) and (9), it can be assumed that the enhanced responsively was obtained owing to (i) higher TCR and/or (ii) higher resistance (more specifically, resistivity in the thinner wire), thus relaxing the trade-off between them.[26,31]

In addition to responsivity, the sensitivity of the microbolometer (any detector system in general) was measured by NEP, which is the input power with a signal-to-noise ratio of one, for the bandwidth of the output noise per unit.[38] NEP is expressed as the smallest measurable power of the microbolometer per the square root of the bandwidth and is calculated by the ratio of noise voltage to responsivity.[39,40] In general, it is the measure of the weakest detectable signal that needs to be as low as possible. The noise power spectrum was measured for the microbolometer with the thermistor

with DW = 0.1 μm at a bias current I_b of 50 μA and for the microbolometer with the thermistor with DW = 0.2 μm at bias currents I_b of 50 and 100 μA in light of the 3% rise in resistance due to heating as the limiting bias current. The detailed theory underlying the measurement and setup has been discussed previously.[33] In the case of responsivity, a constant current (CC) load was connected to the resistance R_T of the thermistor. However, during noise measurement, a metal-film resistor R_L as the load was connected because the constant current load was very noisy. Furthermore, the voltage noise for a constant current load, including noise sources, was calculated based on the circuit diagram in Fig. 4(a), and noise voltage with the CC load was estimated based on the circuit diagram in Fig. 4(b).[33] The measured power spectrum density (PSD) of the

voltage noise with $R_L = 10\,k\Omega$ and the estimated PSD of the voltage noise with the CC load are shown for the device with the thermistor with DW = 0.2 μm at $I_b = 100\,\mu$A in Fig. 4(c), with DW = 0.2 μm at $I_b = 50\,\mu$A in Fig. 4(d), and for the device with the thermistor with DW = 0.1 μm at $I_b = 50\,\mu$A in Fig. 4(e). The characteristics of this noise have been discussed in detail before.[33] The measured and estimated noise was moderately higher than the theoretical values, possibly due to imperfections in the metal wires and the applied bias current. NEPs were calculated from the estimated voltage noise at 10 Hz and responsivity for devices with thermistors with different DWs at different I_b. For devices with the thermistor with DW = 0.1 μm, NEP = $1.85 \times 10^{-10}\,W/\sqrt{Hz}$ (at $I_b = 50\,\mu$A). For devices with the thermistor with DW = 0.2 μm, the NEP was 2.24×10^{-10} (at $I_b = 50\,\mu$A). Moreover, for the same devices (with the thermistor with DW = 0.2 μm), NEP = 1.58×10^{-10} (at $I_b = 100\,\mu$A). Devices with thermistors of different widths at a bias current of 50 μA had

similar NEP values even though the power of voltage noise was high for the high-resistance (DW = 0.1 μm) device. The NEP values of the devices substantially improved in comparison with our previous reports.[26,27,30,31]

Table I gives a comparison between the results obtained here and those of related work in the literature. Note that the devices using VO_x or VO_2 as sensing material (thermistor) recorded higher responsivity owing to higher (bulk) TCR. However, these materials are not naturally abundant and cost-effective and cannot be simply integrated into silicon circuits or compatible with the available semiconductor manufacturing technologies. Although exact comparison is not possible with related work due to differences in structure and measurement conditions, meander structure thermistors have previously been proposed. A study by Saxena *et al.*[36] is similar to the one here, where they used a short meander structure with DW = 2 μm (approximately 10–20 times thicker than the
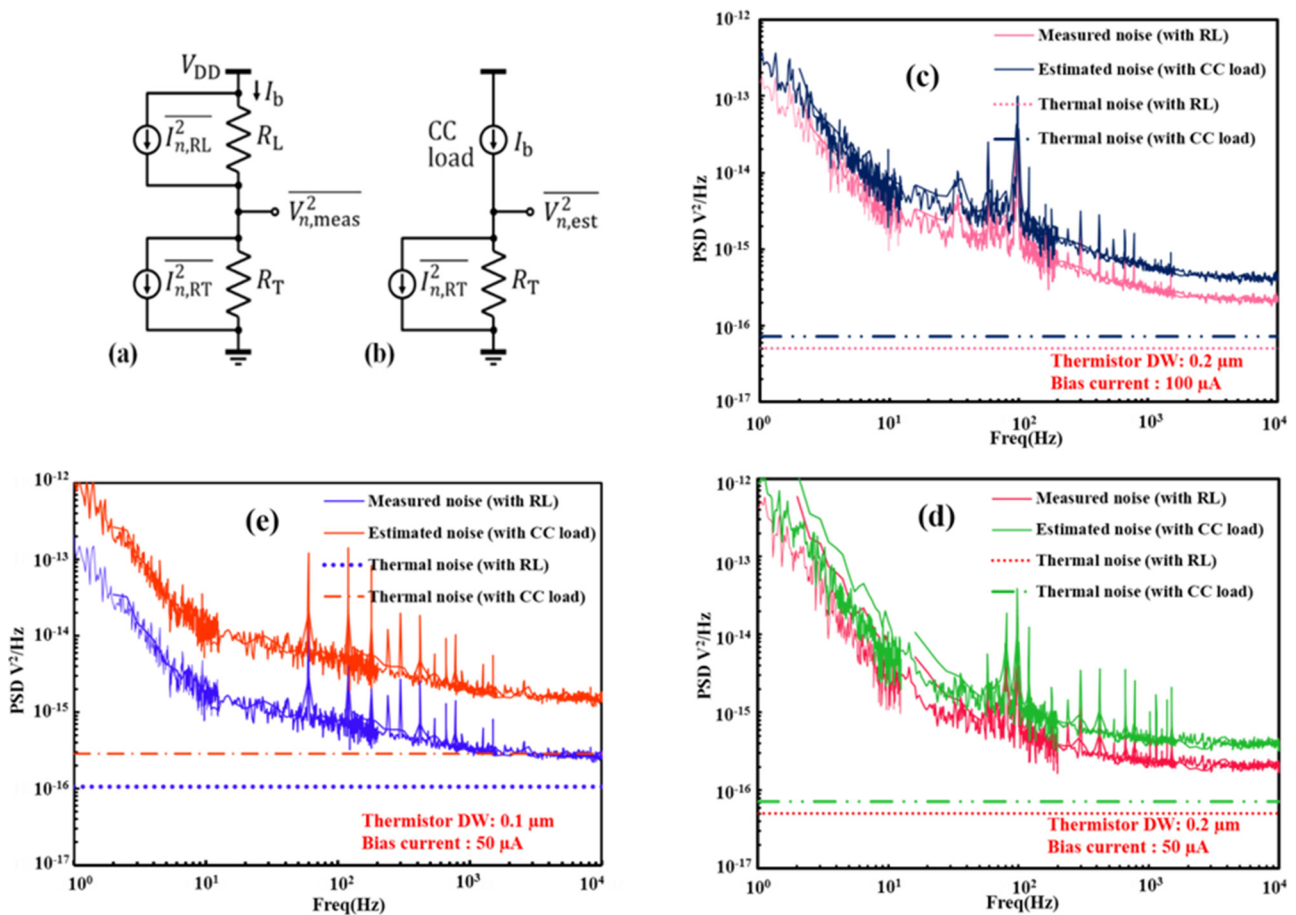
FIG. 4. (a) Circuit diagram of noise measurement, including noise source. (b) Circuit diagram for estimating noise corresponding to responsivity measurement. In the noise measurement, a metal-film resistor was used as load resistor R_L instead of constant current (CC) load because the available CC source was noisy, and the only responsivity was measured using CC load. The power spectrum density (PSD) of voltage noise $\overline{V^2_{n,meas}}$ measured by the circuit (a) with $R_L = 10\,k\Omega$ and that of the $\overline{V^2_{n,est}}$ estimated for (b) with CC load and thermistor R_T of the microbolometer. (c) and (d) Noise PSD for DW = 0.2 μm calculated at $I_b = 100\,\mu$A and 50 μA. (e) Noise PSD for DW = 0.1 μm calculated at $I_b = 50\,\mu$A.

TABLE I. Comparative performance of devices.

S. No.	Detector type	Responsivity (V/W)	NEP (W/Hz$^{1/2}$)	Detector array size	TCR thermistor (%/K)	Reference
1	Absorber-type VO$_x$	12.6 k	…	32 × 32	−1.9	24
2	Absorber-type polycrystal-mixed thin VO$_x$ film	9 k	1.67×10^{-11}	…	−1.5	53
3	Absorber-type thin VO$_x$ film	5 k	…	64 × 2	−0.02	54
4	Absorber-type thin VO2 film	17 k	…	…	…	55
5	Absorber-type Ti	1.6 k	…	256 × 256	0.26	56
6	Half-wave antenna-coupled Ti	90	4.6×10^{-10}	…	0.03	26
7	Polycrystalline SiGe	975	…	…	…	57
8	Absorber-type Ti	30 (meander DW = 2 μm)	…	16 × 16	0.27	58
9	Half-wave dipole antenna-coupled Ti	787 (meander DW = 0.1 μm)	1.85×10^{-10} (electrical)	Unit device	0.16	Current work

thermistor lines in the devices used here) with a unit responsivity of only 30 V/W. The microbolometer devices made in this study with nanometer-width Ti meander thermistors formed in an array stand out in terms of performance of the unit device and scope for further miniaturization. These devices are well suited to state-of-the-art semiconductor fabrication technology and have significant potential for application as on-chip integrable detector arrays. A few related studies on terahertz imaging and sensing can also be highlighted here for a comprehensive understanding of imaging using these devices. However, owing to different structures, measurement parameters, and conditions, they may not be directly comparable with the devices used here. (i) Nemoto et al.[41] dealt with a microbolometer array with a resonant cavity and fabricated a real-time broadband THz camera with high sensitivity. The film microbolometer and thin metallic layer were composed of VO$_x$ and TiAlV, respectively. (ii) Oden et al.[42] dealt with the imaging of broadband terahertz beams using an array of room-temperature antenna-coupled microbolometers. A detailed review of research on THz ICs and implementations of THz imaging and sensing using silicon-based components was conducted by Hillger et al.[43] and may be extremely useful.

The meander shape does not at present improve NEP, and the important merit of our design is higher responsivity. Hence, these devices may not be adequate for thermal imaging with acceptable integration times.[44] However, the device arrays can be still employed in imaging systems that utilize an active THz source, similar to the examples above.[41–43]

A comprehensive model of the narrow-width effect of TCR for metal interconnects is not yet available and may require the consideration of several sources of electron scattering (electron–phonon interactions, electron defects or impurities between electron surfaces, interfaces like grain boundaries, free surfaces), the impact of grain size,[45,47] and the dependence of the electrical resistivity of thin metal films on thickness.[45–51] However, this report helps enhance the understanding of this by establishing a correlation between the device parameters (responsivity and noise) and considers the aspects of design (thermistor width) and the material parameters (TCR, resistivity, and grain size). Note that the enhancement of responsivity in the devices was obtained largely due to the nanoscale meander design that, however, was detrimental to the noise response of the devices. A reduction in DW does not lead to an improvement in NEP. Hence, the key merit of our design is the higher responsivity of

TABLE II. Trend of scaling for microbolometer when thermal conductance is fixed (i.e., thermal conductance of the heater dominates).

Parameters		Scaling factor	Remarks
Thermistor resistance	R_{th}	λ	Increased by factor λ due to meander shape
Thermal conductance	G_{th}	1	Kept constant by the conductance of heater, whose resistance was fixed at resonance resistance for a half-wave dipole antenna
Bias current	I_b	$1/\lambda^{1/2}$	To obtain a fixed ΔT
Bias power consumption	P_b	1	$R_{th} \times I_b^2$
Temperature rise by bias current	ΔT	1	P_b/G_{th} kept constant to assure reliability. This was the primary requirement
TCR of thermistor	α_{th}	1	Properties of the material were assumed independent of the meander shape. In practice, they were slightly reduced due to the narrow-width effect
Responsivity	R_v	$\lambda^{1/2}$	$R_{th} \times I_b \times \alpha_{th}/G_{th}$
Noise voltage	V_{n_th}	$\lambda^{1/2}$	$(4 \times k_B \times T \times R_{th})^{1/2}$, thermal noise was assumed to be dominant.
Noise-equivalent power	NEP	1	V_{n_th}/R_v

TABLE III. Trend of scaling for microbolometer when thermal conductance is inversely proportional to thermistor resistance (R_{th}).

Parameters		Scaling factor	Remarks
Thermistor resistance	R_{th}	λ	Increased by factor λ due to meander shape
Thermal conductance	G_{th}	$1/\lambda$	Inversely proportional to R_{th} based on the assumption that the heater was similarly scaled to the thermistor
Bias current	I_b	$1/\lambda$	To implement fixed ΔT
Bias power consumption	P_b	$1/\lambda$	$R_{th} \times I_b^2$
Temperature rise by bias current	ΔT	1	P_b/G_{th}, kept constant to assure reliability. This was the primary requirement
TCR of thermistor	α_{th}	1	Properties of the material were assumed independent of the meander shape. In practice, they were slightly reduced by the narrow-width effect
Responsivity	R_v	λ	$R_{th} \times I_b \times \alpha_{th}/G_{th}$
Noise voltage	V_{n_th}	$\lambda^{1/2}$	$(4 \times k_B \times T \times R_{th})^{1/2}$, thermal noise was assumed to be dominant
Noise-equivalent power	NEP	$1/\lambda$	V_{n_th}/R_v

these devices along with their compatibility with state-of-the-art semiconductor fabrication technology, which provides scope for their use as on-chip integrable detector arrays. A detailed investigation of the scaling of electrical noise, though important, was not considered here. The trend of scaling, i.e., dimensional characteristics (length dependences) of the electrical responsivity and cutoff frequency of the integrated thermistor and heater for the microbolometer, was studied explicitly in our previous reports for straight metal thermistors.[30,31] Here, the trend of scaling for the meander-shaped antenna-coupled bolometer is provided in Tables II and III. The case (Table II) where thermal conductance was fixed, i.e., the thermal conductance of the heater dominated, was close to the conditions in this study (no improvement in NEP). Improved responsivity relaxes the requirement on the readout circuit, i.e., input-referred noise of the preamplifier can be larger, leading to a smaller footprint and lower power consumption of the preamplifier. In future work, we will seek to further improve responsivity and reduce the NEP and power consumption. This can be accomplished if thermal conductance is inversely proportional to thermistor resistance R_{th} (Table III). To implement this, the resistance of the heater, i.e., resonance resistance of the antenna, should be increased by using a different antenna design. For example, the resonance resistance of the half-wave dipole antenna can be quadrupled if a folded-dipole antenna is used. In addition to its high resistance to resonance, the bandwidth of the antenna is another important factor to be considered because it is related to the minimum detectable change in the temperature of the object, i.e., noise-equivalent temperature difference (NETD). Some reports have suggested the possibility of simultaneously attaining high resistance and large bandwidth.[52]

IV. CONCLUSIONS

This report considered the fabrication of microbolometer arrays with nanometer-sized meander-shaped Ti thermistors to detect terahertz (THz) waves. The aim was to help understand the narrow-width effect in thin metal interconnects by studying how it influences the TCR and resistivity of the metal thermistor and, hence, the final performance of the detectors in terms of electrical responsivity

and NEP. A higher TCR is good for detector performance but is compromised in lower-dimensional devices in the context of efforts to miniaturize detectors. The reduced grain size in thinner metal thermistors was found to be linked to a reduction in TCR and an increase in the resistivity of the devices. The authors found that a thermistor with DW = 0.1 μm is better in terms of electrical responsivity than that with DW = 0.2 μm. The effect of lowering TCR was minimized owing to higher resistivity for the thermistor with DW = 0.1 than that with DW = 0.2 μm. Moreover, an enhancement in responsivity was primarily obtained owing to the nanoscale meander design that, however, was detrimental to the noise response of the devices. These devices with nanoscale meander thermistors are compatible with the state-of-the-art medium-scale semiconductor device fabrication processes and are technologically competitive with related devices with commercial application viability. The optical response, which is currently being investigated with a THz source, is expected to show proportional improvement to that in the electrical results reported here and is likely to enrich the overall understanding of these devices.

REFERENCES

[1]P. Martyniuk, J. Antoszewski, M. Martyniuk, L. Faraone, and A. Rogalski, "New concepts in infrared photodetector designs," Appl. Phys. Rev. **1**, 041102 (2014).

[2]R. M. Woodward, B. E. Cole, V. P. Wallace, R. J. Pye, D. D. Arnone, E. H. Linfield, and M. Pepper, "Terahertz pulse imaging in reflection geometry of human skin cancer and skin tissue," Phys. Med. Biol. **47**, 3853 (2002).

[3]M. Nagel, P. H. Bolivar, M. Brucherseifer, H. Kurz, A. Bosserhoff, and R. Buttner, "Integrated THz technology for label-free genetic diagnostics," Appl. Phys. Lett. **80**(1), 154 (2002).

[4]N. Karpowicz, H. Zhong, C. Zhang, K. I. Lin, J. S. Hwang, J. Xu, and X. C. Zhang, "Compact continuous-wave subterahertz system for inspection applications," Appl. Phys. Lett. **86**(5), 054105 (2005).

[5]K. Yamamoto, M. Yamaguchi, F. Miyamaru, M. Tani, M. Hangyo, T. Ikeda, A. Matsushita, K. Koide, M. Tatsuno, and Y. Minami, "Non-invasive inspection of c-4 explosive in mails by terahertz time-domain spectroscopy," Jpn. J. Appl. Phys. **43**, L414 (2004).

[6]K. Kawase, Y. Ogawa, Y. Watanabe, and H. Inoue, "Non-destructive terahertz imaging of illicit drugs using spectral fingerprints," Opt. Express **11**(20), 2549 (2003).

[7]C. Joerdens and M. Koch, "Detection of foreign bodies in chocolate with pulsed terahertz spectroscopy," Opt. Eng. **47**(3), 037003 (2008).

[8]M. Tonouchi, "Cutting-edge terahertz technology," Nat. Photonics **1**, 97 (2007).

[9]P. H. Siegel, "Terahertz technology," IEEE Trans. Microw. Theory Tech. **50**, 910 (2002).

[10]B. S. Williams, "Terahertz quantum-cascade lasers," Nat. Photonics **1**, 517 (2007).

[11]F. Schuster, D. Coquillat, H. Videlier, M. Sakowicz, F. Teppe, L. Dussopt, B. Giffard, T. Skotnicki, and W. Knap, "Broadband terahertz imaging with highly sensitive silicon CMOS detectors," Opt. Express **19**, 7827 (2011).

[12]X. Cai, A. B. Sushkov, R. J. Suess, M. M. Jadidi, G. S. Jenkins, L. O. Nyakiti, R. L. Myers-Ward, S. Li, J. Yan, D. K. Gaskill, T. E. Murphy, H. D. Drew, and M. S. Fuhrer, "Sensitive room-temperature terahertz detection via the photother-moelectric effect in graphene," Nat. Nanotechnol. **9**, 814 (2014).

[13]L. Liu, J. L. Hesler, H. Xu, A. W. Lichtenberger, and R. M. Weikle, "A broadband quasi-optical terahertz detector utilizing a zero bias Schottky diode," IEEE Microw. Wirel. Compon. Lett. **20**, 504 (2010).

[14]G. C. Trichopoulos, H. L. Mosbacker, D. Burdette, and K. Sertel, "A broadband focal plane array camera for real-time THz imaging applications," IEEE Trans. Antennas Propag. **61**, 1733 (2013).

[15]C. M. Watts, D. Shrekenhamer, J. Montoya, G. Lipworth, J. Hunt, T. Sleasman, S. Krishna, D. R. Smith, and W. J. Padilla, "Terahertz compressive imaging with metamaterial spatial light modulators," Nat. Photonics **8**, 605 (2014).

[16]L. Liang et al., "Anomalous terahertz reflection and scattering by flexible and conformal coding metamaterials," Adv. Opt. Mater. **3**(10), 1311 (2015).

[17]D. B. But, C. Drexler, M. V. Sakhno, N. Dyakonova, O. Drachenko, F. F. Sizov, A. Gutin, S. D. Ganichev, and W. Knap, "Nonlinear photoresponse of field effect transistors terahertz detectors at high irradiation intensities," J. Appl. Phys. **115**, 164514 (2014).

[18]X. Yang, A. Vorobiev, A. Generalov, M. A. Andersson, and J. Stake, "A flexible graphene terahertz detector," Appl. Phys. Lett. **111**, 021102 (2017).

[19]X. Huang, T. Leng, M. Zhu, X. Zhang, J. Chen, K. Chang, M. Aqeeli, A. K. Geim, K. S. Novoselov, and Z. Hu, "Highly flexible and conductive printed graphene for wireless wearable communications applications," Sci. Rep. **5**, 18298 (2014).

[20]J. Noh, M. Jung, Y. Jung, C. Yeom, M. Pyo, and G. Cho, "Key issues with printed flexible thin film transistors and their application in disposable RF sensors," Proc. IEEE **103**, 554 (2015).

[21]A. Rogalski and F. Sizov, "Terahertz detectors and focal plane arrays," Opto Electron. Rev. **19**, 346 (2011).

[22]M. V. S. Ramakrishna, G. Karunasiri, P. Neuzil, U. Sridhar, and W. J. Zeng, "Highly sensitive infrared temperature sensor using self-heating compensated microbolometers," Sens. Actuators A **79**, 122 (2000).

[23]F. Niklau, C. Vieider, and H. Jakobsen, "MEMS/MOEMS technologies and applications III," Proc. SPIE **6836**, 68360D (2007).

[24]S. Chen, H. Ma, S. Xiang, and X. Yi, "Fabrication and performance of microbolometer arrays based on nanostructured vanadium oxide thin films," Smart Mater. Struct. **16**, 696 (2007).

[25]A. Tiwari, H. Satoh, M. Aoki, M. Takeda, N. Hiromoto, and H. Inokawa, "Analysis of microbolometer characteristics for antenna-coupled terahertz detectors," Asian J. Chem. **25**, S358 (2013).

[26]N. Hiromoto, A. Tiwari, M. Aoki, H. Satoh, M. Takeda, and H. Inokawa, "Room-temperature THz antenna-coupled microbolometer with a Joule-heating resistor at the center of a half-wave antenna," in *39th International Conference Infrared, Millimeter, and Terahertz Waves (IRMMW-THz)* (IEEE, 2014), p. R3/A-27.6.

[27]M. Aoki, M. Takeda, and N. Hiromoto, in Proceedings of the International Conference on Global Research and Education (Inter-Academia), Budapest, Hungary, 27–30 August 2012 (Inter Academia, 2012).

[28]A. Tanaka, S. Matsumoto, N. Tsukamoto, S. Itoh, K. Chiba, T. Endoh, A. Nakazato, K. Okuyama, Y. Kumazawa, M. Hijikawa, H. Gotoh, T. Tanaka, and N. Teranishi, "Infrared focal plane array incorporating silicon IC process compatible bolometer," IEEE Trans. Electron Devices **43**, 1844 (1996).

[29]Y. L. Cheng, B. J. Wei, F. H. Shih, and Y. L. Wang, "Stability and reliability of Ti/TiN as a thin film resistor," ECS J. Solid State Sci. Technol. **2**, Q12 (2013).

[30]A. Tiwari, H. Satoh, M. Aoki, M. Takeda, N. Hiromoto, and H. Inokawa, "Fabrication and analytical modeling of integrated heater and thermistor for antenna-coupled bolometers," Sens. Actuators A **222**, 160 (2015).

[31]A. Tiwari, H. Satoh, M. Aoki, M. Takeda, N. Hiromoto, and H. Inokawa, "THz antenna-coupled microbolometer with 0.1-μm-wide titanium thermistor," Int. J. ChemTech Res. 7, 1019 (2015).

[32]A. Banerjee, H. Satoh, A. Tiwari, C. Apriono, E. T. Rahardjo, N. Hiromoto, and H. Inokawa, "Width dependence of platinum and titanium thermistor characteristics for application in room-temperature antenna-coupled terahertz microbolometer," Jpn. J. Appl. Phys. **56**, 04CC07 (2017).

[33]A. Banerjee, H. Satoh, D. Elamaran, Y. Sharma, N. Hiromoto, and H. Inokawa, "Optimization of narrow width effect on titanium thermistor in uncooled antenna-coupled terahertz microbolometer," Jpn. J. Appl. Phys. **57**, 04FC09 (2018).

[34]A. Banerjee, H. Satoh, Y. Sharma, N. Hiromoto, and H. Inokawa, "Characterization of platinum and titanium thermistors for terahertz antenna-coupled bolometer applications," Sens. Actuators A **273**, 49–57 (2018).

[35]J. Lewis, "Far-infrared and sub-millimeter microbolometer detectors," Ph.D. dissertation (University of Texas at Austin, 1994), see http://www.weewave.mer. utexas.edu/MED_files/MED_research/microbolometers/microblmtr_anlys/bolo_ respnsvty.html.

[36]R. S. Saxena, R. K. Bhan, P. S. Rana, A. K. Vishwakarma, A. Aggarwal, K. Khurana, and S. Gupta, "Study of performance degradation in titanium microbolometer IR detectors due to elevated heating," Infrared Phys. Technol. **54**(4), 343 (2011).

[37]S. Zhang, Y. Yang, S. M. Sadeghipour, and M. Asheghi, "Thermal characterization of the 144 nm GMR layer using microfabricated suspended structures," in *Proceedings of ASME Summer Heat Transfer Conference, Las Vegas, Nevada, 21–23 July 2003* (ASME, 2003).

[38]S. Leclercq, see http://www.iram.fr/~leclercq/Reports/About_NEP_photon_ noise.pdf for "Discussion About Noise Equivalent Power and Its Use for Photon Noise Calculation."

[39]P. L. Richards, "Bolometers for infrared and millimeter waves," J. Appl. Phys. **76**, 1 (1994).

[40]V. Mackowiak, J. Peupelmann, Y. Ma, and A. Gorges, see https://www. thorlabs.co.jp/images/TabImages/Noise_Equivalent_Power_White_Paper.pdf for "NEP—Noise Equivalent Power."

[41]N. Nemoto, N. Kanda, R. Imai, K. Konishi, M. Miyoshi, S. Kurashina, T. Sasaki, N. Oda, and M. Kuwata-Gonokami, "High-sensitivity and broadband, real-time terahertz camera incorporating a microbolometer array with resonant cavity structure," IEEE Trans. Terahertz Sci. Technol. **6**, 175 (2016).

[42]J. Oden, J. Meilhan, J. Lalanne-Dera, J. F. Roux, F. Garet, J. L. Coutaz, and F. Simoens, "Imaging of broadband terahertz beams using an array of antenna-coupled microbolometers operating at room temperature," Opt. Express **21**, 4817 (2013).

[43]P. Hillger, J. Grzyb, R. Jain, and U. R. Pfeiffer, "Terahertz imaging and sensing applications with silicon-based technologies," IEEE Trans. Terahertz Sci. Technol. **9**, 1 (2019).

[44]C. Dietlein, A. Luukanen, F. Meyer, Z. Popovic, and E. Grossman, "Phenomenology of passive broadband terahertz images," in *Proceedings of the 4th ESA Workshop on Millimetre-Wave Technology and Applications* (VTT, Helsinki, 2006), pp. 405–410.

[45]V. Barnat, D. Nagakura, P. I. Wang, and T. M. Lu, "Real time resistivity measurements during sputter deposition of ultrathin copper films," J. Appl. Phys. **91**, 1667 (2002).

[46]G. Schindler, G. Steinlesberger, M. Traving, and M. Engelhardt, "Comprehensive study of the resistivity of copper wires with lateral dimensions of 100 nm and smaller," J. Appl. Phys. **97**, 023706 (2005).

[47]Q. Huang, C. M. Lilley, M. Bode, and R. Divan, "Surface and size effects on the electrical properties of Cu nanowires," J. Appl. Phys. **104**, 023709 (2008).

[48]Y. Kitaoka, T. Tono, S. Yoshimoto, T. Hirahara, S. Hasegawa, and T. Ohba, "Direct detection of grain boundary scattering in damascene Cu wires by nanoscale four-point probe resistance measurements," Appl. Phys. Lett. **95**, 052110 (2009).

[49]Y. Hanaoka, K. Hinode, K. Takeda, and D. Kodama, "Increase in electrical resistivity of copper and aluminum fine lines," Mater. Trans. **43**(7), 1621 (2002).

[50]L. L. Melo, A. R. Vaz, M. C. Salvadori, and M. Cattani, "Grain sizes and surface roughness in platinum and gold thin films," J. Metastable Nanocrystalline Mater. **623**, 20 (2004).

[51]M. E. Day, M. Delfino, J. A. Fair, and W. Tsai, "Correlation of electrical resistivity and grain size in sputtered titanium films," Thin Solid Films **254**(1), 285 (1995).

[52]H. Iizuka, T. Watanabe, K. Sakakibara, and N. Kikuma, "Stub-loaded folded dipole antenna for digital terrestrial TV reception," IEEE Antennas Wirel. Propag. Lett. **5**, 260–261 (2006).

[53]C. Chen, X. Yi, J. Zhang, and X. Zhao, "Linear uncooled microbolometer array based on VOx thin films," Infrared Phys. Technol. **42**(2), 87–90 (2001).

[54]H. Wang, X. Yi, G. Huang, J. Xiao, X. Li, and S. Chen, "IR microbolometer with self-supporting structure operating at room temperature," Infrared Phys. Technol. **45**(1), 53–57 (2004).

[55]C. Chen, X. Yi, X. Zhao, and B. Xiong, "Characterizations of VO_2-based uncooled microbolometer linear array," Sens. Actuators A **90**(3), 212–214 (2001).

[56]H.-K. Lee, J.-B. Yoon, E. Yoon, S.-B. Ju, Y.-J. Yong, W. Lee, and S.-G. Kim, "A high fill-factor infrared bolometer using micromachined multilevel electrothermal structures," IEEE Trans. Electron Devices **46**(7), 1489–1491 (1999).

[57]Bjorn F. Andresen and Gabor F. Fulop, Proc. SPIE, **5406**, 521 (2004).

[58]R. Sahai Saxena, R. K. Bhan, P. S. Rana, A.-K. Vishwakarma, A. Aggarwal, K. Khurana, and S. Gupta, "Study of performance degradation in titanium microbolometer IR detectors due to elevated heating," Infrared Phys. Technol. **54**(4), 343–352 (2011).